Molecular dynamics of pyrene based discotic liquid crystals confined in nanopores probed by incoherent quasielastic neutron scattering

ARTICLE *in* RSC ADVANCES · NOVEMBER 2014

Impact Factor: 3.84 · DOI: 10.1039/c4ra13032d

RSC Advances

PAPER

Cite this: *RSC Adv.*, 2014, **4**, 59358

Molecular dynamics of pyrene based discotic liquid crystals confined in nanopores probed by incoherent quasielastic neutron scattering

Makha Ndao,[ab] Ronan Lefort,*[a] Carole V. Cerclier,[ac] Rémi Busselez,[ad] Denis Morineau,[a] Bernhard Frick,[e] Jacques Ollivier,[e] Andriy V. Kityk[f] and Patrick Huber[g]

Semiconducting nanowires made of discotic columnar liquid crystals can be obtained by impregnation into solid nanoporous templates, and provide new opportunities to tailor devices for organic electronics with promising charge carriers transport properties. These properties are tightly related to the self-assembly and molecular dynamics of the discotic columns inside the nanowires. We recently studied and rationalized the formation of different nanostructures in the columnar phase of pyrene derivative discotics nanoconfined in anodic alumina and porous silicon templates ([Cerclier *et al.*, *J. Phys. Chem. C*, 2012, **116**, 18990–18998, Kityk *et al.*, *Soft Matter*, 2014, **10**, 4522–4534]). We now present the molecular dynamics of nano-confined pyrene derivative mesogenic phases as studied by incoherent quasielastic neutron scattering over a broad range of correlation times. The combination of backscattering and time-of-flight techniques has allowed to describe the nature of the molecular motions at play on the pico to nanosecond time scale. The dynamics of the columnar phase is dominated by fluctuations of the lateral chains, while the onset of larger amplitude motions like whole-body reorientations and slow center-of-mass translational diffusion occurs at high temperature in the isotropic phase. Interestingly, nano-confinement does not qualitatively alter the nature of the molecular dynamics, but essentially blocks the long range translational motions and induces broader distributions of correlation times of the fastest local relaxations.

Received 29th September 2014
Accepted 4th November 2014

DOI: 10.1039/c4ra13032d

www.rsc.org/advances

1 Introduction

Discotic columnar liquid crystals (DCLC) are organic materials able to self-arrange into mesogenic columnar orders in a defined temperature range.[1–4] This ability is due to the usually planar disc-like geometry of the molecule, ensured by a rigid polyaromatic core surrounded by soft functional branches (usually simple alkyl tails).[5–10] These discotic molecules tend to form an isotropic liquid phase at high temperature, and stack on top of each other in columns at lower temperatures. The columns also self-assemble into a highly orientationally ordered hexagonal lattice,[11,12] that nevertheless does not exhibit translational order along the column axis because of the liquid-like mobility of the flexible branched chains that fill in the inter-columnar space. This liquid crystalline structural stacking is accompanied by a strong overlap of the aromatic π electronic orbitals, that propagates along the columns and gives rise to long-range transport of charge-carriers. This one dimensional charge transfer pathways confer to DCLC materials unique properties suitable for new organic electronic applications. In particular, their exceptional charge mobility and short lived excitonic response compared to conductive polymers has raised considerable interest on DCLC based devices such as molecular transistors or solar cells.[5,13–19]

Up to now, the electronic and structural properties of bulk or thin film materials have been extensively studied on typical discotics such as triphenylene and hexa-*peri*-hexabenzocoronene (HBC) derivatives.[20–23] Recently, our group has also focused on a new generation of pyrene based DCLCs.[15,24–27]

Clearly, applicability of DCLC in operational devices strongly relies on the control of their growth into large monodomains. Usually, columns exhibit planar (edge-on) alignment in open thin films, while they align homeotropically when sandwiched

[a]*Institut de Physique de Rennes (IPR), UMR-CNRS 6251, Université de Rennes 1, Campus de Beaulieu, 35042 Rennes, France. E-mail: ronan.lefort@univ-rennes1.fr*
[b]*Institut de Chimie de Clermont-Ferrand (ICCF) – UMR-CNRS 6296, Université Blaise Pascal, Campus des Cézeaux, 63171 Aubiere Cedex, France*
[c]*Institut des Matériaux Jean Rouxel (IMN), Université de Nantes, CNRS, 2 rue de la Houssiniere, BP32229, 44322 Nantes Cedex 3, France*
[d]*Institut des Molécules et Matériaux du Mans, UMR-CNRS 6283, Université du Maine, 72085 Le Mans Cedex 9, France*
[e]*Institut Laue-Langevin (ILL), 71 avenue des Martyrs, 38000 Grenoble, France*
[f]*Faculty of Electrical Engineering, Czestochowa University of Technology, 42-200 Czestochowa, Poland*
[g]*Institute of Materials Physics and Technology, Hamburg University of Technology (TUHH), D-21073 Hamburg-Harburg, Germany*

between two solid substrates.[28,29] Some strategies have been proposed to control macroscopic orientations of the domains in thin films, especially with a focus on the homeotropic alignment compatible with usual solar cell geometries.[30–38]

Recently, DCLC nanowires have been proposed as an alternative to thin films for organic photovoltaic applications, assuming the columns will align with the nanowires axis, and provide efficient one dimensional semiconducting nano-objects.[39] Steinhart and co-workers have demonstrated the possible formation of such DCLC nanowires by impregnation of the liquid crystal in anodic alumina oxide[40] (AAO) porous layers used as templates.[41] Such nanowires have a diameter from 30 nm to 60 nm and a length about 70 μm (length of the template pores). However, the nature of the columnar order over large scales remains questionable in these systems, as the final DCLC self-assembly can be strongly altered by several coexisting and competing effects due to the nano-confinement in the AAO template (anchoring energy at the pore surface, finite size cut-offs to correlation lengths, thermodynamic Gibbs–Thomson shifts of phase transitions…).[24,42–44]

In addition to these structural aspects, the molecular mobility in columnar phases is also a physical property of utmost relevance. Indeed, it is widely admitted that the time scale of molecular motions and that of the charge carriers transport should overlap, therefore strongly influencing the conductivity of the DCLC structure.[16,45–48] Although the molecular motions in the different phases of discotic mesogens have been studied using a large panel of complementary experimental techniques including quasielastic neutron scattering coupled to computer simulations,[46–50] broadband dielectric spectroscopy,[25,26,51–53] NMR[54,55] or optical Kerr effect,[56] the general features of this molecular dynamics still appear rather complex, especially because of a coexistence of simple molecular modes promoted by the high orientational order in the columns with a more glassy structural dynamics fostered by the disorder and flexibility of the branched chains in the inter-columnar space.[26,47,49,50,53,57,58]

In the present paper, we report on the molecular dynamics of the DCLC $Py(CEH)_4$ (pyrene 1,3,6,8 tetra-*rac*-2-ethylhexyl tetracarboxylate) nanowires confined in the nanopores of AAO or porous silicon templates, analysed by quasielastic incoherent neutron scattering (QENS). QENS is one of the only experimental techniques which response can be measured over a range of correlation times from 10 ps to 10^4 ps (thanks to the combination of backscattering and time of flight techniques), and allowing for the characterization of all types of molecular relaxations, from long range translational motions to local chain ends fluctuations. Neutrons also present the advantage of being fully transferred through the AAO solid templates without significant scattering, then allowing for a focus on the confined DCLC response. In a first part, we detail the reference results in the different phases of the bulk $Py(CEH)_4$. In a second part, this bulk reference is compared to the results obtained on $Py(CEH)_4$ confined in nanopores. In both cases, the temperature dependence is discussed in terms of effective mean square displacements and the same qualitative models of motion are used to analyse the QENS response in the frequency domain, in order to emphasize the effect of nano-confinement in templates.

2 Materials and methods

2.1 Discotic columnar liquid crystals

The discotic liquid crystal $Py(CEH)_4$ (pyrene 1,3,6,8 tetra-*rac*-2-ethylhexyl tetracarboxylate) was synthesized and purified at the Centre de Recherche Paul Pascal (CRPP) at Bordeaux, France. This compound shows a stable columnar hexagonal phase over an extended temperature range between 225 K and 375 K.[25,32,59]

Although competitive electronic properties are obtained with other DCLC, this prototypical molecule has been selected for its stable columnar order near room temperature.

2.2 Nanoporous membranes

2.2.1 Anodized aluminium oxide (AAO) membranes. AAO nanoporous membranes were synthesized at the Institut de Physique de Rennes from annealed aluminium foils (purity: 99.99%) provided by Alfa Aesar. Samples were first cleaned with acetone and then electro-polished in a solution of ethanol and perchloric acid (60%) (75 : 25). Afterwards, a double anodization was performed in a thermally isolated electro-chemical cell under constant voltage. The main parameters involved in anodization are the output voltage, the electrolyte composition, and the temperature.[40,56,60,61] The parameters used here to obtain pores of diameter either 25 or 50 nm (standard deviation: 5 nm) were given elsewhere.[24]

2.2.2 Nanoporous silicon. Porous silicon layers were produced from polished p^+-type (100) oriented silicon substrates (300 μm thick, 3 inch diameter, 0.003 Ω to 0.007 Ω). Silicon wafers were electrochemically etched in a solution of ethanol mixed with hydrofluoric acid (20%) (60 : 40), using a platinum working electrode and an electrochemical cell under constant current of 240 mA. The final pore diameters were *c.a.* 8 nm. Etching was achieved for two hours to obtain 100 μm thick porous layers.

2.2.3 Confinement. $Py(CEH)_4$ was confined into nanoporous samples by spontaneous imbibition in the isotropic liquid phase. Membranes were dried at 403 K under vacuum for several hours prior to use. Then, filling was achieved under $Py(CEH)_4$ vapour pressure in a vacuum chamber at a temperature of 403 K, above the Col_h–Iso transition, in order to accelerate the filling of the pores by capillary action. The excess of liquid crystal was removed by squeezing the samples between Whatman filtration papers.

2.3 Neutron quasielastic scattering experiments

2.3.1 Sample details and data preparation. For all experiments, the samples were sealed in slab aluminium containers of internal thickness of either 1 or 2 mm. The sample plane was oriented at 135° with respect to the incident beam. The experimental resolution was measured at temperatures below 5 K on the sample itself. These low temperature data were also used for intensity normalization. Standard data corrections (empty cell subtractions, self-absorption, energy rebinning and constant Q

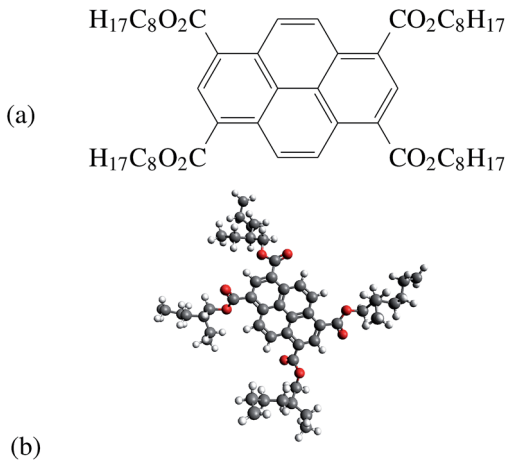

Fig. 1 (a) Chemical structure of the Py(CEH)$_4$ molecule (pyrene 1,3,6,8 tetra-*rac*-2-ethylhexyl tetracarboxylate), and (b) its 3D representation in a random conformation.

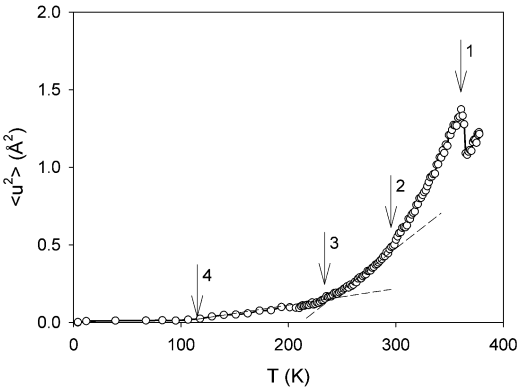

Fig. 2 Mean square displacement of bulk Py(CEH)$_4$. Arrows point to particular dynamical crossovers (see text). Dashed lines are guides to the eye.

interpolation for time of flight data) were applied using conventional software suites provided by the ILL (Lamp macros, SQW and SQWel tools). The final datasets consist in collections of incoherent dynamic structure factors $S(Q, \omega)$. These functions are usually modelled as the sum of an elastic and a quasielastic contributions:[62]

$$S(Q, \omega) = A(Q)\delta(\omega) + [1 - A(Q)]f_q(Q, \omega) \quad (1)$$

The normalized intensity $A(Q)$ of the elastic peak is referred to as the elastic incoherent structure factor (EISF), and the description of both the EISF $A(Q)$ and the quasielastic part $f_q(Q, \omega)$ requires a molecular or phenomenological model of local motions. The fitting of quasielastic models to the experimental data (convoluted by the experimental resolution) has been achieved using the STR_fit module of the ILL Lamp program.

2.3.2 Backscattering (BS) experiments. High resolution quasielastic spectra and elastic temperature scans were measured on the IN16 spectrometer at the Institut Laue Langevin (ILL) in Grenoble. A monochromatized beam with a center wavelength $\lambda = 6.271$ Å is sent to the sample *via* a 14 Hz oscillating mirror (Doppler machine) and Si(111) analyser crystals in backscattering geometry. The final energy resolution obtained is better than 1 μeV (FWHM) over an energy window of *c.a.* ±15 μeV. When the Doppler machine is turned off, only neutrons that are elastically scattered within the experimental resolution are counted. The temperature dependence $I_{el}(Q, T)$ of this fixed energy window count will be commonly referred to as an 'elastic scan'. In the harmonic approximation of vibrations, this elastic intensity is described by the Debye–Waller factor

$$I_{el}(Q, T) \sim \exp\left(-\frac{Q^2\langle u^2\rangle}{3}\right) \quad (2)$$

where the mean square displacement (MSD) $\langle u^2\rangle(T)$ often follows a linear behaviour *versus* temperature. If relaxational motions are present, this approximation breaks down whereas an effective MSD can still be extracted by eqn (2). In this case, a crossover is observed in its temperature dependence.

2.3.3 Time of flight (TOF) experiments. Standard TOF data were acquired in the energy range up to ~100 meV on the cold high flux disk chopper apparatus IN5B at the ILL, at a wavelength of 8 Å, corresponding to a typical energy resolution about 30 μeV FWHM.

3 Dynamics of bulk Py(CEH)$_4$

3.1 Effective mean square displacement

The MSD of bulk Py(CEH)$_4$ is displayed in Fig. 2. It is extracted from the Q dependence of the elastic intensity measured on cooling using the BS spectrometer IN16, according to eqn (2).

At high temperatures above the clearing point, the occurrence of large amplitude isotropic relaxational processes leads to a complete breakdown of the Debye–Waller approximation, and the measured MSD reaches physically meaningless values. The Iso–Col$_h$ first order transition (arrow #1) corresponds to the sudden freezing of some isotropic motions, evidenced as a discontinuity in the MSD curve.

Below the clearing point, in the columnar phase, the MSD shows a highly non linear variation, with a smooth although marked change around room temperature (arrow #2 in the figure). This second crossover appears gradual on cooling and reminiscent of the non linear behaviour of $\langle u^2\rangle(T)$ observed in many soft matter systems, and assigned to the freezing (glass transition) of dynamical degrees of freedom occurring on the time scale of the BS experiment.[63] This glass-like behaviour has been reported as a characteristic dynamic feature of the columnar phase in DCLC triphenylene and coronene core compounds,[26,48,50–52,57,58,64,65] and usually assigned to the freezing of the uni-axial molecule rotation around the column axis. Evidence of glassy dynamics has also been reported on faster time scales in the columnar[50] or isotropic phase[56] of triphenylene compounds. Experimental indications of similar features in Py(CEH)$_4$ have also been reported recently.[25]

A third crossover around 220 K corresponds to the crystallization of the columnar phase (see Fig. 1), and a fourth one

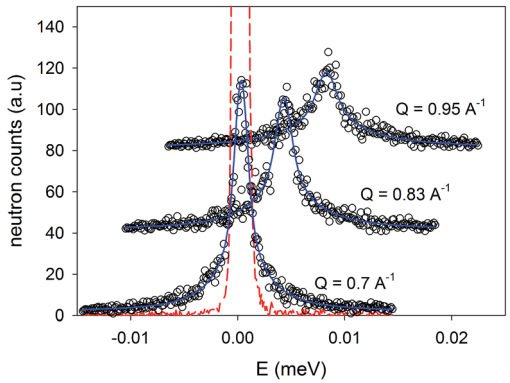

Fig. 3 Quasielastic spectra measured at 380 K in the isotropic phase of bulk Py(CEH)$_4$ for different values of the momentum transfer (IN16 backscattering data). The dashed line is the spectrum of the sample at 2 K, that shows the experimental resolution function. The solid lines are the best fits obtained with two Lorentzian functions (see text).

around 110 K indicates the freezing of low amplitude relaxational motions in the solid state. Such observation in this temperature range is typical of methyl groups rotations, as observed in many systems as diverse as polymers[66,67] or biomolecules.[68]

At low temperatures, the MSD becomes very low and linearly dependent on T, as expected for a harmonic solid.

3.2 Bulk isotropic phase

The Fig. 3 displays typical quasielastic spectra measured on the BS spectrometer IN16 in the isotropic phase of bulk Py(CEH)$_4$. No elastic contribution to scattering is observed on this experimental space time scale. This is a direct indication that long range translational self diffusion is an active process within the time scale defined by the BS instrumental resolution.[62] However, the quasielastic line shape cannot be reproduced by a single Lorentzian line, indicating that these translational motions are more complex than a simple random walk, or more likely that other dynamical processes are also at play.

The data were best fitted using two Lorentzian lines. The assignment of these two components to physical processes is not unique and model dependent. In particular, inhomogeneous situations can exist where all the scatterers (here mainly protons) might be involved in different motions (*e.g.* molecular cores or tails). However, one of the simplest interpretation relies on the assumption that all the scatterers are both involved in two independent motions: translational diffusion and a second localized process[43,62] (molecular isotropic rotation, libration, *etc.*). Adopting this point of view, the scattering law can be described as the convolution product of a Lorentzian line f_1 of half width at half maximum (HWHM) Γ_1 modelling self diffusion with a second law modelling a localized process with an elastic contribution balanced with a quasielastic component f_r (also assumed to be Lorentzian with HWHM Γ_r):

$$\begin{aligned} S(Q,\omega) &= \exp\left(-\frac{Q^2\langle u^2\rangle}{3}\right) f_1(Q,\omega,\Gamma_1) \otimes [A(Q)\delta(\omega) \\ &\quad + (1-A(Q)) f_r(Q,\omega,\Gamma_r)] \\ &= \exp\left(-\frac{Q^2\langle u^2\rangle}{3}\right) A(Q) f_1(Q,\omega,\Gamma_1) \\ &\quad + \exp\left(-\frac{Q^2\langle u^2\rangle}{3}\right)(1-A(Q)) \times f_2(Q,\omega,\Gamma_2=\Gamma_1+\Gamma_r) \end{aligned} \quad (3)$$

where f_1 and f_r are unitary functions, Γ_1 and Γ_2 are the experimental line widths and $A(Q)$ the EISF of the localized processed (see eqn (1)), and the experimental quasielastic line $f_2 = f_1 \otimes f_r$ remains a unitary Lorentzian shape. The experimental values of Γ_1 and Γ_r are shown in Fig. 4.

Γ_1 shows a clear linear evolution with Q^2. This behaviour is compatible with standard translational diffusion with diffusion coefficient D. In that case, the scattering law is purely Lorentzian with a HWHM that obeys $\Gamma = DQ^2$.[62] In the present case, the slope at low Q of Γ_1 gives $D \simeq 10^{-11}$ m^2 s^{-1}. This value of D is in very good agreement with the one reported for triphenylene compounds by PFG NMR experiments probing the diffusion motion on the micrometer length scale.[54]

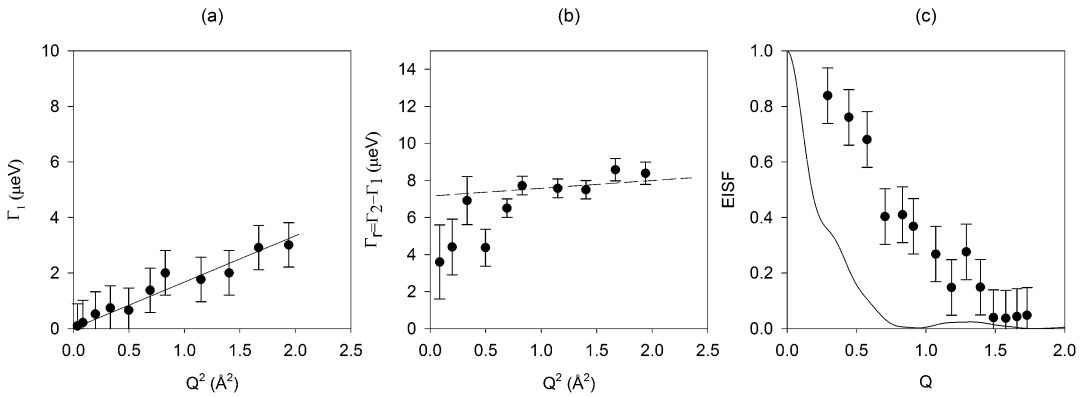

Fig. 4 Half width at half maximum of the two Lorentzian functions fitting the BS data on bulk Py(CEH)$_4$ in the isotropic phase. (a) FWHM of the line assigned to the translational diffusion process; (b) FWHM and (c) EISF of the line assigned to a second localized process. The solid line in (c) represents an average theoretical EISF expected for isotropic rotation of the molecule.

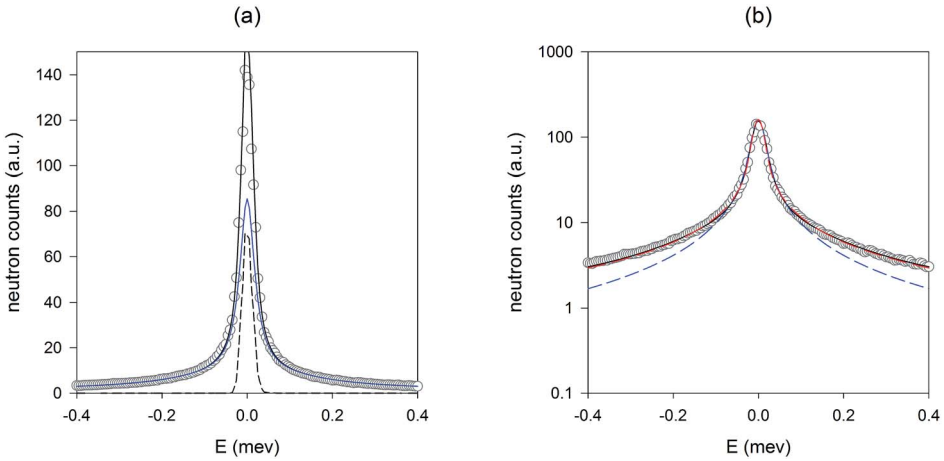

Fig. 5 Quasielastic spectrum measured at 380 K in the isotropic phase of bulk $Py(CEH)_4$ at $Q = 1.1$ Å^{-1} (IN5B time of flight data). (a) Best fit with one elastic peak and a sum of Lorentzian lines (model A); (b) best fit of model A (black solid line) compared to best fits of stretched exponential Fourier transforms (model B) with parameter $\beta = 0.43$ (blue dashed line) and $\beta = 0.2$ (red dashed line). Models A and B with $\beta = 0.2$ are virtually indistinguishable.

Γ_r essentially does not depend on Q within the experimental window, and remains close to 7 μeV (equivalent relaxation time $\simeq$190 ps). This observation is compatible with simple localized molecular motions like isotropic reorientation, which is known from NMR experiments to be much faster than the μs time range.[11,55] The EISF expected for the isotropic rotation of a single scatterer is given by the spherical Bessel function of 0th order $A(Q) = j_0^2(QR)$, where R is the distance of the scatterer from the centre of rotation. For $Py(CEH)_4$, the protons can be located between 3.5 (molecule core) and 12.5 Å (lateral chain ends) from the molecule centre (depending on the extent of folding of the lateral chains). The theoretical EISF averaged over these two limits is shown Fig. 4(c). It is compared with the experimental one, which can be simply obtained as the integrated intensity I_1 of the quasielastic line associated to translation divided by the total integrated spectrum intensity, *i.e.* $A(Q) = \frac{I_1}{I_1 + I_2}$. It is obvious that the experimental EISF is much larger than expected. This excess of elastic intensity indicates that isotropic reorientations are not fully experimentally described within the BS window. In the present case, these full rotations are too fast to be completely captured within the BS window, and part of the quasielastic integral is not measured. This therefore leads to an overestimation of the EISF.

In order to have a better insight into the nature of these fast local relaxations, TOF measurements were carried out at 380 K in the isotropic phase of bulk $Py(CEH)_4$ (Fig. 5). This TOF response differs significantly from the backscattering one. Over a broad Q range, it contains a strong contribution, the linewidth of which is resolution limited, together with a quasielastic contribution which is not a single Lorentzian. Qualitatively, this TOF response is very similar to QENS measurements reported by Kearley and co-workers on triphenylene compounds.[46,47] These authors have discussed two complementary interpretations of their data: the first one assuming that the TOF signal results from the superposition of different local dynamical processes associated with scatterers involved in distinct molecular groups (model A). It results in a scattering law obeying eqn (1) including a true elastic peak that describes the localized character of the observed motions. The second interpretation disregards the geometrical details of the dynamics but takes into account a distribution of correlation times (model B) through a phenomenological description of the scattering law. The data are then described in the time domain (intermediate scattering function $I(Q, t)$) and compared to stretched exponential decays $I(Q,t) \propto \exp\left(-\left(\frac{t}{\tau}\right)^{\beta}\right)$.[50,69] This model assumes a fractional but long range diffusion process occurring on the time scale of the TOF experiment, and therefore does not contain a true elastic contribution. As a consequence, models A and B are not equivalent.

We have applied both approaches in order to determine which one does describe TOF data measured on $Py(CEH)_4$ at best. The comparison of models A and B is shown on Fig. 5. Model A was completed using an elastic peak in addition to a quasielastic contribution (both shown on Fig. 5(a)). Three Lorentzian lines were needed to describe correctly this latter contribution. Model B was tested over a broad range of the parameter β. As shown in Fig. 5(b), best fits were obtained only for $\beta = 0.2$ (or even lower at small Q). This values appear unphysically low for bulk isotropic liquid systems. Fits using more realistic values of β are unable to reproduce the experimental observations at high energy (see in Fig. 6(b) an example of fit with $\beta = 0.43$, a value that has been proposed to describe the fast dynamics of triphenylene derivatives[50]). As a consequence, we ruled out model B and have considered that the TOF data on $Py(CEH)_4$ actually contain a genuine elastic contribution.

The presence of this finite elastic intensity indicates that large scale translational motions are slower than the experimental resolution, in full agreement with the BS results.

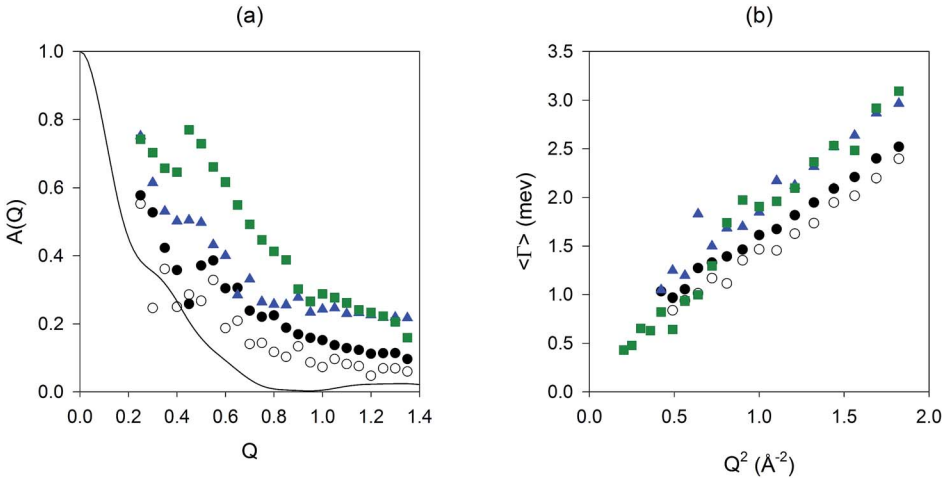

Fig. 6 (a) EISF of the quasielastic response measured by TOF in the isotropic phase of bulk $Py(CEH)_4$ (open circles), $Py(CEH)_4$ confined in anodic aluminium oxide membranes of pore diameter of 50 (solid circles) and 25 nm (triangles), on confined in porous silicon (squares). These data are compared to the same model of isotropic rotation as discussed for BS data. (b) Average quasielastic FWHM of the TOF response in the isotropic phase of $Py(CEH)_4$, bulk or confined (same symbol code). Error bars have been omitted for clarity: typical orders of magnitude are ± 0.1 for the EISF and ± 100 μeV for the quasielastic linewidth.

Similarly, these BS results have shown that large amplitude molecular rotations are also slower than the TOF resolution. As a consequence, the TOF quasielastic response must be interpreted in terms of both shorter time and length scale fluctuations, for instance core librations and branched chains reorientations.

The choice of the number of lines and of their Lorentzian shape needed to describe the quasielastic part of our data appeared essentially arbitrary, and tentative assignments of these lines to well defined relaxation modes are irrelevant without the help of complementary information (*e.g.* light scattering experiments or molecular dynamics simulations). This simple approach allows however for an unambiguous determination of the elastic incoherent structure factor of the TOF response. This EISF is displayed as black dots in Fig. 6(a).

This EISF remains low, below 0.2 for all Q values larger than 0.5 $Å^{-1}$. This an indirect indication that the amplitude of the motions detected within the TOF time scale is still significant.

The three Lorentzian lines used in the fitting procedure were found of comparable integrated intensity, and with FWHM of respectively 0.031, 0.29 and 3.2 meV at $Q = 1$ $Å^{-1}$ (resp. 42, 4.5 and 0.4 ps). These three lines likely reflect a more complex or even continuous distribution of correlation times (heterogeneous superposition of different dynamic processes involving same and/or different scatterers in the molecule), but it is interesting enough to underline that the slower process (42 ps) is not so far from the fastest characterized by BS measurements (190 ps). We then might tentatively assign the slower processes observed in the TOF data to the onset of isotropic molecular rotations (probably not completed on the time scale of TOF QENS). This idea is supported by the experimental EISF which is much closer now to the theoretical one expected for isotropic reorientations (see Fig. 6(a), the experimental excess of elastic intensity at high Q could be explained by the fact that this time, part of the quasielastic response is slower than the TOF resolution).

The characteristic FWHM of the quasielastic response is displayed *versus* Q^2 for bulk $Py(CEH)_4$ as black dots in Fig. 6(b). It was defined as the average of the Lorentzian components line widths weighted by their relative integrated intensity (eqn (4)).

$$\langle \Gamma \rangle = \frac{\sum_i I_i \Gamma_i}{\sum_i I_i} \tag{4}$$

The individual line widths Γ_i range between 30 μeV (~44 ps) and 3 meV (~0.4 ps) at $Q = 1$ $Å^{-1}$. These values are comparable to these reported on triphenylene compounds in the vicinity of the clearing point.[46,48]

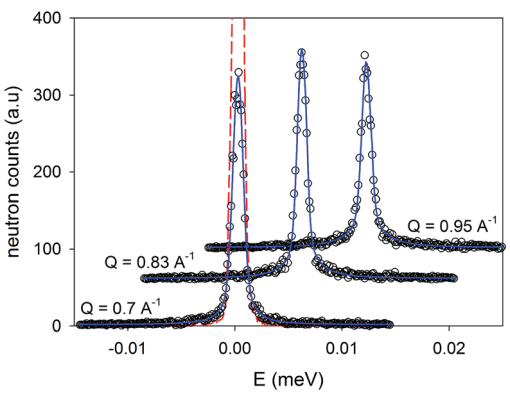

Fig. 7 Quasielastic spectra measured at 300 K in the columnar phase of bulk $Py(CEH)_4$ for different values of the momentum transfer (IN16 backscattering data). The resolution function is shown (dashed line). The solid lines are the best fits obtained with one elastic and one Lorentzian functions (see text).

Opposite to the BS data, the behaviour of this line width is clearly dispersive, suggesting at least a partial delocalized nature of the molecular dynamics. The contribution of lateral functional chains might appear here dominant. This observation is in fair agreement with data previously reported on triphenylene compounds,[50] where the authors proposed a model of dispersive kinetics[70] to describe the molecular dynamics in the columnar phase and interpret its main characteristics in terms of long-time scale correlations between rare events in the side-chains dynamics and slow molecular cores motions. As discussed above, this point of view cannot directly be transposed in our case to the isotropic phase of $Py(CEH)_4$, due to the reminiscence of a pure elastic peak.

3.3 Bulk columnar phase

The BS QENS response measured in the bulk columnar phase of $Py(CEH)_4$ is shown in Fig. 7. Contrary to observations in the isotropic phase, the signal does not become broader with increasing Q, and a strong resolution limited contribution remains. This is a direct indication that long range translational diffusion processes have become much slower that the resolution of the BS experiment ($\sim$1 ns). This is also in agreement with the observed freezing of diffusion processes (with D dropping down to $\sim 10^{-14}$ m^2 s^{-1}) at the isotropic to columnar phase transition, observed on other similar compounds using PFG NMR.[54]

The data were then fitted using a simple model according to eqn (1) with $f_q(Q, \omega)$ chosen as a single Lorentzian line (see eqn (3)). The quantitative results are shown in Fig. 8. The EISF (Fig. 8(a)) appears much higher that observed in the isotropic phase, and the line width (Fig. 8(b)) is clearly non dispersive, with an average FWHM around 2.5 μeV ($\sim$530 ps). Here again, these features are consistent with a simple image of localized molecular motions of significant amplitude. The structure of the columnar phase rules out isotropic molecular rotations, but suggests uni-axial rotations around the main molecular axis (aligned with the column axis). ^{13}C NMR experiments have shown that these motions are much faster than the μs time scale in the vicinity of the clearing point.[11,55] As a guide for the eye, our experimental data are compared with the theoretical powder averaged EISF expected for a single scatterer undergoing a uni-axial rotation (averaged over radii $r = 3.5$ and $r = 12.5$ Å). As an evidence, the experimental data are much higher than theoretically expected. Dielectric spectroscopy measurements on $Py(CEH)_4$ have evidenced the occurrence of the main reorientational relaxation at a peak frequency within 10^6 Hz to 10^8 Hz in the temperature domain of the columnar phase.[26] This frequency range is indeed faster than the lower bound indicated by NMR, but appears too slow to give rise to a quasielastic response out of the BS resolution.

As a consequence, the BS response observed in the columnar phase of $Py(CEH)_4$ more likely arises from two phenomena. The first one implies limited out-of-plane motions of the discs inside the columns[51] (in the case of triphenylene compounds, these out-of-plane tumblings have been shown to be of small amplitude[11,55]). The second one is due to a part of the strong and heterogeneous contribution of the different protons located on the lateral chains, which may undergo fast localized fluctuations. But part of the quasielastic scattering associated to these lateral chains motions seems again to be broader than the BS window.

These dynamical processes should be associated to the second crossover observed in the temperature dependence of the mean square displacement (see Fig. 2). As discussed above in section 3.1, this crossover represents a glassy dynamical freezing. In agreement with the dielectric experiments, we then suggest that the plastic columnar phase of the $Py(CEH)_4$ molecular cores retains all characteristics of a uni-axial orientational glass former, while the columns inter-spaces are occupied by the lateral chains which also experience glassy dynamics.

A typical TOF spectrum measured in the columnar phase is shown in Fig. 9. Here again, the data clearly show the evidence of a purely elastic peak. We then analysed the data using a similar model as for the isotropic phase (two Lorentzian lines were here enough to achieve the same quality of fit). The EISF (Fig. 10(a)) is here also higher than the one measured above the clearing point (see Fig. 6(a)). The average line width was defined in a similar way as for the isotropic phase (see eqn (4)), and its Q dependence is displayed in Fig. 10(b). On the contrary to the

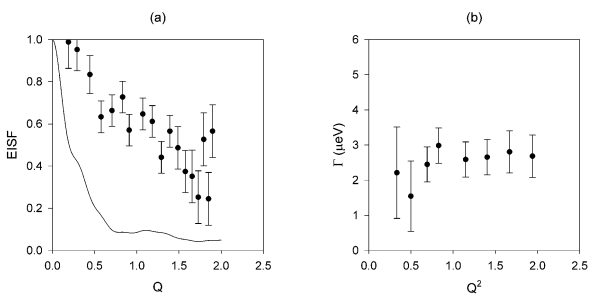

Fig. 8 (a) Backscattering elastic incoherent structure factor and (b) quasielastic line width (FWHM) measured at 300 K in the columnar phase of bulk $Py(CEH)_4$. The solid line in (a) is the powder averaged theoretical EISF expected for a single scatterer undergoing a uni-axial rotation (see text).

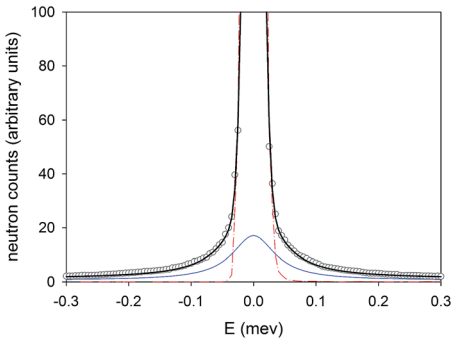

Fig. 9 Time of flight spectrum measured at 300 K in the columnar phase of $Py(CEH)_4$ at $Q = 0.65$ Å^{-1}. The solid black line is the best fit using the model described in the text, including an elastic peak (red dashed line), and a quasielastic peak (blue solid line).

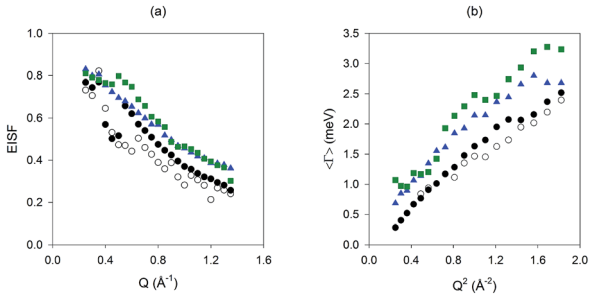

Fig. 10 (a) EISF of columnar Py(CEH)$_4$ at $T = 300$ K for the bulk (open circles), or confined in AAO 50 nm (solid circles), AAO 25 nm (triangles) or in porous silicon (squares); (b) average TOF quasielastic line width (same symbol code).

EISF and to the BS data, the average relaxation times seem hardly affected by the phase transition. This enforces the hypothesis that the dominant quasielastic contribution in TOF data arises from lateral chains motions, that can be much less affected by the columnar orientational ordering than the molecular cores are expected to be. These combined observations suggest that the nature of the motions at play remain similar in both phases, but experience a significant reduction of their amplitude below the clearing point temperature.

4 Dynamics of Py(CEH)$_4$ confined in nanopores

The quasielastic response of confined Py(CEH)$_4$ is shown in Fig. 11. The BS spectra measured in the isotropic phase display qualitative features that contrast with the response of the bulk liquid crystal: they appear essentially resolution limited, with a very low intensity quasielastic broadening at the bottom of the elastic component. Clearly, the slow translational motions that were accessible in the BS data for the bulk become now slower

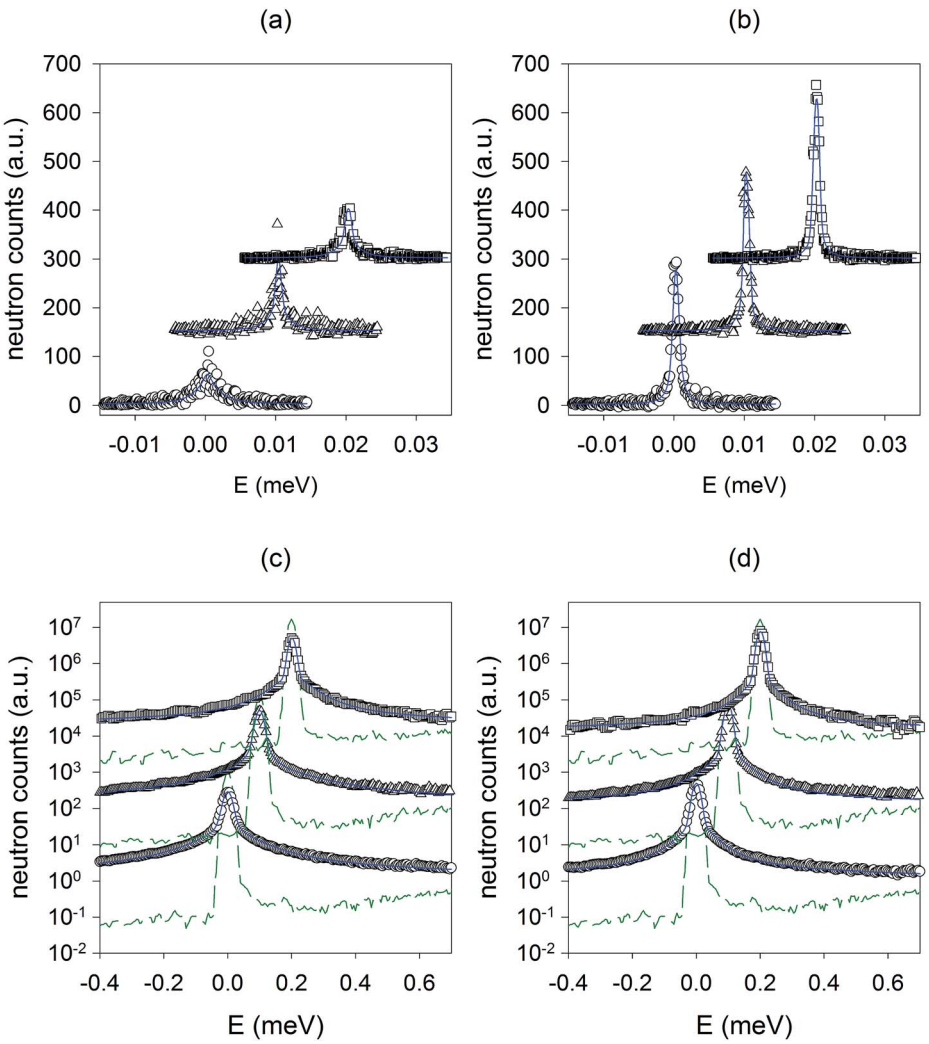

Fig. 11 Quasielastic spectra measured at $Q \simeq 0.9$ Å^{-1} on Py(CEH)$_4$ confined in AAO membranes of 50 nm and 25 nm (resp. circles and triangles) and in porous silicon (squares) by backscattering (a and b) and time of flight (c and d) techniques, at 380 K in the isotropic phase (a and c), and 300 K in the columnar phase (b and d). The TOF spectra are shown on a logarithmic scale together with the experimental resolution function (dashed line). For all spectra, the solid line represents the best fit to the experimental data (see text).

than the experimental resolution under confinement. Also the higher energy quasielastic broadening that was present in the bulk data fades out in the nanoporous membranes. The low signal to noise ratio prevents a confident quantitative analysis of this latter contribution, but an immediate comparison of the BS spectra at 380 K and 300 K reveals that this overall low scattering intensity observed in the isotropic phase is due to a strong effective Debye–Waller factor. This suggests indirectly that large amplitude motions remain under confinement, which frequency exceeds the BS window.

This is indeed confirmed by the TOF response in the confined isotropic phase (Fig. 11(c)), that shows the presence of a strong quasielastic broadening in the meV range. In both the isotropic and columnar phases, the TOF spectra display the same qualitative features as for the bulk: an elastic component together with a broad quasielastic contribution, that can be well reproduced by the sum of two (columnar phase) or three (isotropic phase) Lorentzian lines. The quantitative analysis of the associated EISF and average quasielastic line widths for the confined samples are comparatively displayed in Fig. 6 and 10. First of all, no major difference compared to the bulk has to be noticed in the Q dependence of these quantities. Especially, the same dispersive character of the average line width is observed. Also, the same relative increase of the EISF is seen on cooling below the clearing point, while in the meantime the average line width remains essentially the same (again same behaviour as the bulk).

Both Fig. 6(a) and 10(a) reveal a significant increase of the EISF for confined $Py(CEH)_4$ over the whole range of momentum transfer Q. Although this effect is marked in both phases, it seems relatively more pronounced in the isotropic phase. We might tentatively interpret this observation as an average restriction of the amplitude of molecular relaxations induced by the confinement. However, this point of view can only be partial, as the measured EISF cannot be associated to a single relaxational process but rather to an heterogeneous distribution of intramolecular motions, as discussed in the preceding section. The interpretation of the observed EISF as a simple Fourier transform of scatterers trajectories is therefore over-simplified. Nevertheless, it is consistent with the general idea that confinement introduces a liquid–solid interface where molecules of the confined phase might experience a severe reduction of some orientational or translational degrees of freedom, either through a direct interaction with the solid surface or more indirectly through collective interfacial effects, as already reported in other glass forming liquids or calamitic mesogens.[42,71,72]

This increase of the elastic contribution goes along with a small although clear broadening of the average quasielastic response in the confined samples compared to the bulk (see Fig. 6b and 10b). Almost bulk-like in the 50 nm alumina matrix, this broadening seems to scale with the pore size for smaller pores. This observation of an acceleration of the molecular motions in confinement is rather unusual, and might be intimately linked with changes in the local structure or entanglement of the lateral chains of the molecules as suggested by the EISF behaviour, and that should affect the local activation energy barriers and their distributions.

5 Discussion and conclusion

The combination of BS and TOF data has allowed to evidence that the confinement of the discotic liquid crystal at the nano scale does not modify deeply the nature of the molecular dynamics at play within the QENS relaxation times window. This dynamics appears to be dominated by fluctuations of the lateral chains, with the onset of larger amplitude motions like whole-body reorientations and slow center-of-mass translational diffusion at high temperatures in the isotropic phase.

Confinement effects on the molecular dynamics then express themselves as a second order quantitative shortening of the relaxation times of localized motions, together with a blocking of slow large amplitude motions. This stretching of the dynamical range both towards slower and faster tails of the distribution compared to the bulk is in agreement with observations reported on other systems.[42,50,72] However, in the present case, this point of view of a heterogeneous stretching of relaxation times distributions induced by confinement hardly captures the whole physical parameters responsible for the observations, as other structural features very specific to discotic mesogens especially in the columnar phase might also play a crucial role. Indeed, the structure of $Py(CEH)_4$ has been thoroughly studied by our group, and reported in the different alumina and silicon porous membranes in a previous paper.[24] It has been shown that two main aspects of the DCLC structure are strongly affected by the confinement: (i) the thermodynamic equilibrium temperatures are in a classical way shifted downwards, in association with a smearing of the transition zones and the emergence of hysteresis phenomena, (ii) the homeotropic anchoring is privileged at the DCLC/porous matrix interface, and promotes a radial rather than planar ordering of the columns with respect to the pore axis. Even in the smallest

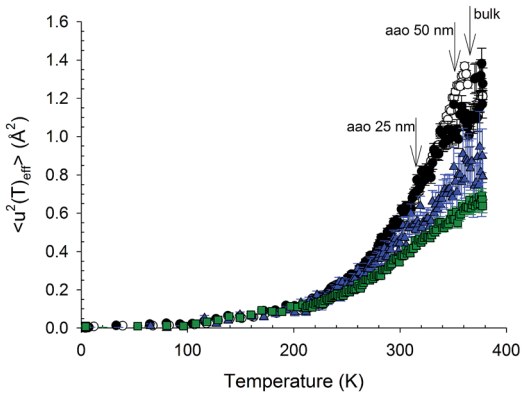

Fig. 12 Mean square displacement measured on $Py(CEH)_4$ using the IN16 backscattering spectrometer in the bulk (open circles) or confined in alumina membranes of 50 (solid circles) and 25 nm (solid triangles) pore diameters, and porous silicon (solid squares). The clearing points of the different samples, determined independently, are marked by the arrows.

pores and on the length scale comparable to the static correlation length, the radial defected columnar ordering is not much distorted compared to the defect-free bulk structure. The local orders at the molecular scale are therefore very similar, at least not different enough to affect significantly the molecular dynamics.

On the other hand, the phase diagram is strongly affected by confinement, and the temperature at which the QENS spectra were measured can be from one system to another relatively differently separated from the thermodynamical events such as crystallization or clearing point. The Fig. 12 illustrates this situation, through the temperature dependence of the MSD measured within the resolution of BS on the confined systems (for sake of clarity and comparison, the bulk results of Fig. 2 have been reported). In the crystal phases, below 220 K, the MSDs are the same for all systems and reflect a dynamics dominated by chains ends (methyl groups) rotations. Above, by entering the confined columnar phases, the MSDs start to scale differently depending on the pore size, in agreement with the restriction of motions amplitude in smaller pores deduced from TOF data. But the new information stems from the first crossover that occurs at higher temperatures in the MSD curves (corresponding to the clearing point, see Fig. 2). This clearing point is strongly shifted downwards when the pore size decreases.[24] Due to the coupling of the local molecular dynamics to the structure, this temperature shift leads to differences observed in the QENS responses measured at the same temperature on different systems. The measurements done in the isotropic phase at 380 K were done close to the clearing point for the bulk and the DCLC confined in the 50 nm AAO, but much further away from it in the two other confined samples. Similarly, the measurements done in the columnar phase at 300 K were done close to the apparent glass transition (crossover #3) for the bulk and AAO 50 nm sample, but close to the clearing point for the AAO 25 nm sample. For the porous silicon sample, the clearing point almost vanishes,[24] and only a weak and short range columnar ordering, which order parameter is still not saturated at 300 K. As a consequence, the dynamics of the different samples compared at the same temperature are those of different thermodynamical states with various extents of pre-columnar order at the pores surface.[44] The DCLC confined in the smaller pores appear as if they were at higher temperature (relatively to their clearing point), in a more locally disordered state than the larger pores (or the bulk). Smaller pore samples therefore experience larger distributed (and maybe even lowered) activation energy barriers, which promote effective shorter correlation times, even if the mean square displacement is reduced.

As a conclusion, the semi-quantitative image provided by the QENS experiments on these confined DCLC nanowires results from the interplay of competing effects. First, the surface interaction (anchoring) of the liquid crystals at the pore surface and the pore size (spatial restriction) could both slow down or reduce the amplitude of the dynamics (which is especially observed for the large amplitude motions such as translational dynamics). Second, the structural and thermodynamical effects induce downward shift of the transition temperature and additional disorder (as the homeotropic anchoring in channels induces defective structures). These latter effects could lead to an apparent acceleration of some modes (as observed for the more local motions, alkyl chain and librations).

Acknowledgements

We are grateful to Eric Grelet for stimulating and fruitful scientific discussion. We are also grateful to Julien Kelber and Harald Bock (CRPP) for having synthesized and provided the liquid crystalline material studied here. This work was supported by European FEDER funds, and the French-German project TEMPLDISCO jointly founded by ANR (ANR-09-BLAN-0419) and the German Science foundation (HU 850/3-1). A.V.K. acknowledges financial support by the Polish National Science Centre (NCN) under the Project? Molecular Structure and Dynamics of Liquid Crystals Based Nanocomposites? (Decision no. DEC-2012/05/B/ST3/02782).

References

1 H. K. Bisoyi and S. Kumar, *Chem. Soc. Rev.*, 2010, **39**, 264–285.
2 L. Chen, X. Dou, W. Pisula, X. Yang, D. Wu, G. Floudas, X. Feng, K. Müllen and K. Mullen, *Chem. Commun.*, 2012, **48**, 702–704.
3 S. Kumar, *Isr. J. Chem.*, 2012, **52**, 820–829.
4 S. Sergeyev, W. Pisula and Y. H. Geerts, *Chem. Soc. Rev.*, 2007, **36**, 1902–1929.
5 S. Alibert-Fouet, S. Dardel, H. Bock, M. Oukachmih, S. Archambeau, I. Seguy, P. Jolinat and P. Destruel, *ChemPhysChem*, 2003, **4**, 983–985.
6 S. Alibert-Fouet, I. Seguy, J.-F. Bobo, P. Destruel and H. Bock, *Chem.–Eur. J.*, 2007, **13**, 1746–1753.
7 H. Bock, A. Babeau, I. Seguy, P. Jolinat and P. Destruel, *ChemPhysChem*, 2002, **3**, 532–535.
8 H. Bock, M. Rajaoarivelo, S. Clavaguera and E. Grelet, *Eur. J. Org. Chem.*, 2006, **2006**, 2889–2893.
9 S. Saïdi-Besbes, E. Grelet and H. Bock, *Angew. Chem.*, 2006, **118**, 1815–1818.
10 G. Zucchi, B. Donnio and Y. H. Geerts, *Chem. Mater.*, 2005, **17**, 4273–4277.
11 M. Ndao, R. Lefort, P. Huber, J.-M. Zanotti, B. Frick, A. Schoenhals and D. Morineau, *MRS Proceedings*, 2011, 1349, mrss11–1349–dd02–05.
12 V. Rutar, R. Blinc, M. Vilfan, A. Zann and J. Dubois, *J. Phys.*, 1982, **43**, 761–765.
13 D. Adam, P. Schuhmacher, J. Simmerer, L. Häussling, K. Siemensmeyer, K. H. Etzbachi, H. Ringsdorf, D. Haarer and L. Haussling, *Nature*, 1994, **371**, 141–143.
14 G. Chidichimo and L. Filippelli, *Int. J. Photoenergy*, 2010, **2010**, 123534.
15 T. M. Figueira-Duarte and K. Müllen, *Chem. Rev.*, 2011, **111**, 7260–7314.
16 J.-I. Hanna, A. Ohno and H. Iino, *Thin Solid Films*, 2014, **554**, 58–63.
17 B. R. Kaafarani, *Chem. Mater.*, 2011, **23**, 378–396.

18 I. O. Shklyarevskiy, P. Jonkheijm, N. Stutzmann, D. Wasserberg, H. J. Wondergem, P. C. M. Christianen, A. P. H. J. Schenning, D. M. de Leeuw, Z. Tomović, J. Wu, K. Müllen and J. C. Maan, *J. Am. Chem. Soc.*, 2005, **127**, 16233–16237.

19 L. Cisse, P. Destruel, S. Archambeau, I. Seguy, P. Jolinat, H. Bock and E. Grelet, *Chem. Phys. Lett.*, 2009, **476**, 89–91.

20 S. Ito, M. Wehmeier, J. D. Brand, C. Kübel, R. Epsch, J. P. Rabe and K. Müllen, *Chem.–Eur. J.*, 2000, **6**, 4327–4342.

21 S. K. Pal, S. Setia, B. S. Avinash and S. Kumar, *Liq. Cryst.*, 2013, **40**, 1769–1816.

22 L. Schmidt-Mende, A. Fechtenkötter, K. Müllen, E. Moons, R. H. Friend and J. D. MacKenzie, *Science*, 2001, **293**, 1119–1122.

23 J. Wu, W. Pisula and K. Müllen, *Chem. Rev.*, 2007, **107**, 718–747.

24 C. V. Cerclier, M. Ndao, R. Busselez, R. Lefort, E. Grelet, P. Huber, A. V. Kityk, L. Noirez, A. Schönhals and D. Morineau, *J. Phys. Chem. C*, 2012, **116**(35), 18990–18998.

25 E. Dantras, J. Dandurand, C. Lacabanne, L. Laffont, J. M. Tarascon, S. Archambeau, I. Seguy, P. Destruel, H. Bock and S. Fouet, *Phys. Chem. Chem. Phys.*, 2004, **6**, 4167–4173.

26 C. Krause, H. Yin, C. Cerclier, D. Morineau, A. Wurm, C. Schick, F. Emmerling and A. Schönhals, *Soft Matter*, 2012, **8**, 11115–11122.

27 E. Charlet and E. Grelet, *Phys. Rev. E: Stat., Nonlinear, Soft Matter Phys.*, 2008, **78**, 041707.

28 V. De Cupere, J. Tant, P. Viville, R. Lazzaroni, W. Osikowicz, W. R. Salaneck and Y. H. Geerts, *Langmuir*, 2006, **22**, 7798–7806.

29 O. Karthaus, H. Ringsdorf, V. V. Tsukruk and J. H. Wendorff, *Langmuir*, 1992, **8**, 2279–2283.

30 T. Brunet, O. Thiebaut, E. Charlet, H. Bock, J. Kelber and E. Grelet, *EPL*, 2011, **93**, 16004.

31 E. Grelet and H. Bock, *EPL*, 2006, **73**, 712.

32 E. Grelet, S. Dardel, H. Bock, M. Goldmann, E. Lacaze and F. Nallet, *Eur. Phys. J. E: Soft Matter Biol. Phys.*, 2010, **31**, 343–349.

33 K. Hatsusaka, K. Ohta, I. Yamamoto and H. Shirai, *J. Mater. Chem.*, 2001, **11**, 423–433.

34 W. Pisula, v. Tomović, B. E. Hamaoui, M. D. Watson, T. Pakula and K. Müllen, *Adv. Funct. Mater.*, 2005, **15**, 893–904.

35 E. Pouzet, V. D. Cupere, C. Heintz, J. W. Andreasen, D. W. Breiby, M. M. Nielsen, P. Viville, R. Lazzaroni, G. Gbabode and Y. H. Geerts, *J. Phys. Chem. C*, 2009, **113**, 14398–14406.

36 G. Schweicher, G. Gbabode, F. Quist, O. Debever, N. Dumont, S. Sergeyev and Y. H. Geerts, *Chem. Mater.*, 2009, **21**, 5867–5874.

37 O. Thiebaut, H. Bock and E. Grelet, *J. Am. Chem. Soc.*, 2010, **132**, 6886–6887.

38 E. Charlet, E. Grelet, P. Brettes, H. Bock, H. Saadaoui, L. Cisse, P. Destruel, N. Gherardi and I. Seguy, *Appl. Phys. Lett.*, 2008, **92**, 024107.

39 J. H. Park, M. Labardi and G. Scalia, *Proc. SPIE*, 2014, **9004**, 90040U.

40 L. Ba and W. S. Li, *J. Phys. D: Appl. Phys.*, 2000, **33**, 2527.

41 M. Steinhart, S. Zimmermann, P. Göring, A. K. Schaper, U. Gösele, C. Weder and J. H. Wendorff, *Nano Lett.*, 2005, **5**, 429–434.

42 R. Lefort, D. Morineau and R. Guégan, *Phys. Rev. E: Stat., Nonlinear, Soft Matter Phys.*, 2008, **78**, 040701.

43 R. Lefort, D. Morineau, R. Guegan, E. Al, R. Guégan, C. Ecolivet, M. Guendouz, J.-M. Zanotti and B. Frick, *Phys. Chem. Chem. Phys.*, 2008, **10**, 2993–2999.

44 A. Kityk, M. Busch, D. Rau, S. Calus, C. V. Cerclier, R. Lefort, D. Morineau, E. Grelet, C. Krause, A. Schönhals, B. Frickg, P. Huber, A. V. Kityk, C. V. Cerclier, A. Schonhals and B. Frick, *Soft Matter*, 2014, **10**, 4522–4534.

45 L. A. Haverkate, M. Zbiri, M. R. Johnson, B. Deme, F. M. Mulder and G. J. Kearley, *J. Phys. Chem. B*, 2011, **115**, 13809–13816.

46 G. J. Kearley, F. M. Mulder, S. J. Picken, P. H. J. Kouwer and J. Stride, *Chem. Phys.*, 2003, **292**, 185–190.

47 O. Kruglova, F. M. Mulder, S. J. Picken, J. Stride and G. J. Kearley, *Phys. B*, 2004, **350**, E1003–E1005.

48 F. M. Mulder, J. Stride, S. J. Picken, P. H. J. Kouwer, M. P. de Haas, L. D. A. Siebbeles and G. J. Kearley, *J. Am. Chem. Soc.*, 2003, **125**, 3860–3866.

49 C. Krause, R. Zorn, F. Emmerling, J. Falkenhagen, B. Frick, P. Huber and A. Schonhals, *Phys. Chem. Chem. Phys.*, 2014, **16**, 7324–7333.

50 O. Kruglova, F. M. Mulder, G. J. Kearley, S. J. Picken, J. a. Stride, I. Paraschiv and H. Zuilhof, *Phys. Rev. E: Stat., Nonlinear, Soft Matter Phys.*, 2010, **82**, 51703.

51 M. M. Elmahdy, G. Floudas, M. Kastler and K. Müllen, *J. Phys.: Condens. Matter*, 2008, **20**, 244105.

52 H. Groothues, F. Kremer, D. M. Collard and C. P. Lillya, *Liq. Cryst.*, 1995, **18**, 117–121.

53 C. Krause and A. Schönhals, *J. Phys. Chem. C*, 2013, **117**, 19712–19720.

54 S. V. Dvinskikh, I. Furó, H. Zimmermann and a. Maliniak, *Phys. Rev. E: Stat., Nonlinear, Soft Matter Phys.*, 2002, **65**, 50702.

55 D. Goldfarb, Z. Luz and H. Zimmermann, *J. Phys.*, 1981, **42**, 1303–1311.

56 J. Li, K. Fruchey and M. D. Fayer, *J. Chem. Phys.*, 2006, **125**, 194901.

57 B. Glüsen, A. Kettner, J. Kopitzke and J. Wendorff, *J. Non-Cryst. Solids*, 1998, **241**, 113–120.

58 M. Möller, J. H. Wendorff, M. Werth and H. W. Spiess, *J. Non-Cryst. Solids*, 1994, **170**, 295–299.

59 T. Hassheider, S. A. Benning, H.-S. Kitzerow, M.-F. Achard and H. Bock, *Angew. Chem.*, 2001, **40**, 2060–2063.

60 A. P. Li, F. Müller, A. Birner, K. Nielsch and U. Gösele, *J. Appl. Phys.*, 1998, **84**, 6023–6026.

61 A.-P. Li, F. Müller, A. Birner, K. Nielsch and U. Gösele, *Adv. Mater.*, 1999, **11**, 483–487.

62 M. Bée, *Quasielastic neutron scattering: principles and applications in solid state chemistry, biology, and materials science*, Adam Hilger, 1988.

63 B. Frick and D. Richter, *Science*, 1995, **267**, 1939–1945.
64 S. U. Vallerien, M. Werth, F. Kremer and H. W. Spiess, *Liq. Cryst.*, 1990, **8**, 889–893.
65 Z. Yildirim, M. Wübbenhorst, E. Mendes, S. J. Picken, I. Paraschiv, A. T. M. Marcelis, H. Zuilhof, E. J. R. Sudhälter and E. J. Sudhölter, *J. Non-Cryst. Solids*, 2005, **351**, 2622–2628.
66 K. Chrissopoulou, S. H. Anastasiadis, E. P. Giannelis and B. Frick, *J. Chem. Phys.*, 2007, **127**, 144910.
67 R. Zorn, B. Frick and L. J. Fetters, *J. Chem. Phys.*, 2002, **116**, 845–853.
68 Z. Yi, Y. Miao, J. Baudry, N. Jain and J. C. Smith, *J. Phys. Chem. B*, 2012, **116**, 5028–5036.
69 A. Arbe, J. Colmenero, F. Alvarez, M. Monkenbusch, D. Richter, B. Farago and B. Frick, *Phys. Rev. E: Stat., Nonlinear, Soft Matter Phys.*, 2003, **67**, 51802.
70 Y. A. Berlin, A. L. Burin and S. F. Fischer, *Chem. Phys.*, 1997, **220**, 25–41.
71 R. Guégan, D. Morineau and C. Alba-Simionesco, *Chem. Phys.*, 2005, **317**, 236–244.
72 R. Zorn, L. Hartmann, B. Frick, D. Richter and F. Kremer, *J. Non-Cryst. Solids*, 2002, **307–310**, 547–554.